Iron-Oxide Exsolution an Important Power Source for Earth's Dynamo

Nicholas Knezek Tushar Mittal Chris McGuire
Sarah Arveson Curtis Williams Jackie Li

1 Abstract

Earth has been observed to have a global magnetic field for at least the past 3.5 billion years [Tarduno et al., 2015], but recent high thermal conductivity measurements [Pozzo et al., 2012] and resulting young inner-core ages [Labrosse, 2015] make it difficult to sustain Earth's magnetic field by cooling and inner-core growth alone. Exsolution of light elements such as magnesium [Badro et al., 2016, O'Rourke and Stevenson, 2016] and silicon [Hirose et al., 2017] from Earth's core have been proposed as sources of energy to resolve this problem. We show that exsolution of iron-oxide from the core is an important third source of energy for the dynamo. We create a coupled thermodynamic evolution and chemical interaction model between Earth's core and mantle and show that exsolution of light elements from the core depends heavily on the composition of the background mantle and timescale of mantle convection. We show iron-oxide exsolution is the dominant source of compositional entropy production across a range of plausible parameter choices, with possible implications for the origin of LLSVPs and ULVZs. We also find exsolution reduces the magnitude of increase in available entropy at inner-core nucleation and allows for a wider range of inner-core nucleation times when compared to dynamos powered by cooling, making detection of a paleomagnetic signal of inner-core nucleation more difficult.

2 Introduction

TUSHAR - I'll deal with this section ..

3 Model

We model the thermal evolution of the Earth using a coupled core-mantle thermodynamic model following the methods of Stevenson et al. [1983] for parameterized mantle convection and Nimmo [2015] for core thermodynamics. We add chemical reactions between the core and mantle to this system, modeled as an

interaction layer at the base of the mantle that is allowed to chemically equilibriate with the core fluid. This governs the exsolution of light elements from the core into the mantle, which contribute to the heat and entropy budget of the core. This system is cast as a system of first-order ODEs and solved forward in time from Earth's formation to the present day.

3.1 Chemical Interactions

We model chemical interactions between the core and mantle as a system of equilibrium reactions with the base of the lower mantle. First-principles calculations and seismic observations argue for a pyrolitic lower mantle, necessitating the convesion of minerals such as olivine and ferropericlase transported from the upper mantle into Bridgemanite at depth. While the exact mechanisms of this process are not well understood, it requires interaction between mineral species at relatively large distances over timescales of millions of years. Thus, at long enough timescales the chemical state of the lower mantle should be able to be modeled as an equilibrium reaction system.

A similar argument can be made about core-mantle interactions. Material from the lower mantle can both diffuse into and exolve out of the core, setting up a system of equlibrium reactions. To model this, we assume a typical length-scale for chemical interactions in the mantle and keep track of the moles of each mantle mineral in this layer. There is considerable uncertainty concerning the mechanisms by which Earth's core and mantle interact, and therefore the appropriate length-scale is uncertain. If chemical interaction is dominated by atomic diffusion, interaction length-scales of H$\sim$1-10m over 100 Myr may be appropriate Bina [2010], Van Orman et al. [2003]. If grain-boundary diffusion occurs at the CMB, it could allow H$\sim$100m Hayden and Watson [2007], while H$\sim$1km could be appropriate if core material physically intrudes into the lower mantle [Kanda and Stevenson, 2006].

In our model, we track Fe, Mg, Si, O in the core. These species exchange with the mantle through the equilibrium reactions

$$MgO(mantle) \leftrightarrow Mg^{(met)} + O^{(met)} \tag{1}$$

$$SiO_2(mantle) \leftrightarrow Si^{(met)} + 2O^{(met)} \tag{2}$$

$$FeO(mantle) \leftrightarrow Fe^{(met)} + O^{(met)} \tag{3}$$

as can be seen in figure 1. Each of these reactions is governed by their temperature dependent equilibrium constant. We use the values reported by [Hirose et al., 2017] for SiO2 and FeO and [Badro et al., 2016] for MgO. In our model, we only allow Mg, Si, and O to leave the core, but not enter. An undersaturated core would allow light elements from the mantle to dissolve into the core fluid at the CMB. However, this would form a thin stratified layer at the CMB heavily enriched in light elements which would not easily mix with the bulk of the core and would shut down further dissolution of material [CITE]. Thus, the bulk of the core composition would remain unchanged.

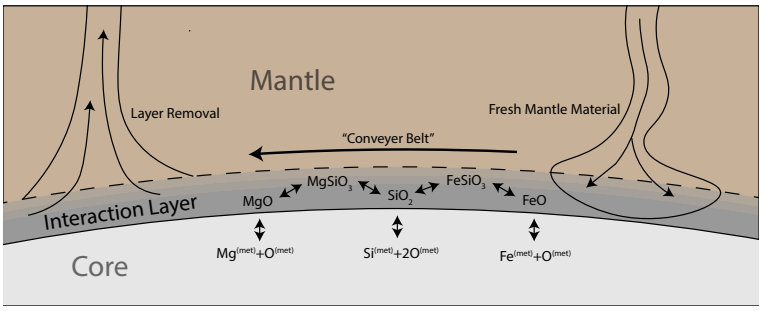

Figure 1: Overview of the dynamics and reactions governing chemical exchange between the core and mantle.

The composition of the mantle interaction layer consists of MgO, SiO_2, FeO, $MgSiO_3$, and $FeSiO_3$. The total number of moles of each species are tracked and governed by the reactions

$$MgSiO_3 \leftrightarrow MgO + SiO_2 \tag{4}$$

$$FeSiO_3 \leftrightarrow FeO + SiO_2 \tag{5}$$

$$FeSiO_3 + MgO \leftrightarrow FeO + MgSiO_3 \tag{6}$$

where the third reaction maintains stoichiometry in the layer and has an equilibrium constant defined as 1. This constrains $K_{(4)}$ to equal $K_{(5)}$. The lower mantle is expected to be mostly Bridgemanite in the present day, so that $K_{(4)} = K_{(5)} \ll 1$.

3.2 Interaction Layer Dynamics

Exsolved material from the core builds up at the base of the mantle over time, altering the composition of the interaction layer and therefore affecting the exsolution of core species. At the same time, the interaction layer moves with the background mantle convection along the free surface of the CMB, setting up a "conveyer belt" system as in figure 1. In this system, the layer is removed by mantle upwellings or plumes and replaced with fresh background mantle due to downwellings or sinking slabs on a timescale τ set by the background mantle convection. Analytical stability analyses and 2D numerical mantle convection codes show that exsolved material in our model never reaches the required thickness and buoyancy contrast to form Rayleigh-Taylor instabilities, in contrast with other recent results [Helffrich et al., 2017].

To model this "conveyer belt" layer overturn, we include a layer erosion term in our system of differential equations that pushes each species towards the background mantle composition value. Assuming a pyrolitic background mantle composition and specifying a layer thickness sets the total number of moles $M_{b,i} $ of each species i in the layer. Our equations are cast in terms of absolute number of moles, so the erosion term $\left(\frac{dM_i}{dt}\right)_{erosion}$ for each species

is a function only of the difference $M_i - M_{b,i}$ and the timescale of layer overturn τ (see supplement).

In our model, we assume a present day τ_p between 200 and 800 Myr. The early earth likely had more vigorous convection, so we set the timescale at early earth $\tau_0 = \tau_p/8$ and set τ at intermediate times using an exponential relationship varying between these values with a timescale of 1 Byr.

We assume a pyrolitic background lower mantle based on seismic an first-principles estimates. This consists of 83% Bridgemanite, 16% ferroperilase, and 1% free SiO2, with a magnesium number of 0.8 [CITE].

3.3 Thermodynamic Model

We model the thermodynamic evolution of Earth's core by modifying the method of Nimmo [2015] to include terms for latent heat release and gravitational energy release for MgO, SiO2, and FeO exsolution. The gravitational energy and entropy released by exsolution is expressed as

$$Q_{g,i} = \int \rho \psi \alpha_i \frac{dc}{dt} dV \,, \qquad E_{g,i} = Q_{g,i}/T_c$$

from Table 1 in that work. This requires an estimate of the compositional expansion α_i for each species. We use $\alpha_{MgO} \sim 0.84$ (O'Rourke, Korenaga 2016) and $\alpha_{SiO2} \sim 1.117$ [Hirose et al., 2017]. For FeO, we perform a simple hard-sphere estimate to compute the change in density between a parcel of fluid with 99 wt% Fe, 1 wt% O and 100 wt% Fe to obtain $\alpha_{FeO} \sim 0.28$.

We compute latent heat release for each species through $Q_{L,i} = L_{H,i} \frac{dm_i}{dt}$, where $\frac{dm_i}{dt}$ is the change in the mass of the species with time and $L_{H,i}$ is the latent heat of exsolution for each species. We use $L_{H,SiO2} = 4300$ kJ/kg [Hirose et al., 2017], while $L_{H,MgO} = L_{H,FeO} = 910$ kJ/kg represents a value intermediate between that for SiO2 and inner-core solidifcation. These value has little effect on the system, as the total heat released by exsolution of light elements is quite small. We find <5% difference in model run outcomes when setting all latent heat of exsolution values to zero. Note also that unlike latent heat from inner-core growth, the latent heat from exsolution does not contribute to the entropy production in the core as heat released at the CMB does not contribute to thermal convection. In fact, latent heat of exsolution has a negative effect on the energy available to power a dynamo because it decreases the core cooling rate.

Chemical exchange between the core and the interaction layer at the base of the mantle causes only small changes to the bulk physical properites of the layer and do not significantly affect mantle dynamics. Therefore, we use a simple 1D parameterized whole-mantle convection model following the method of [Stevenson et al., 1983] to track the mantle temperature evolution over time. We use an Arrhenius mantle viscosity with present day viscosities varying from $\mu_p = 10^{19.5}$ to 10^{21} Pa s. We use Stevenson's values for all parameters except for radiogenic heat production in the mantle, which we replace using the method from **?** which includes four individual radioactive species.

3.4 Coupled Thermodynamic-Chemical System

We couple the chemical evolution equations and the thermodynamic model into a system of first-order ODEs. To do this, we take the derivative of each equilibrium reaction (1) - (6) with respect to temperature. These equations are tightly coupled and highly nonlinear due to the dependence of each equation on both the number of moles of each species and the total number of moles in the core or mantle. Therefore, we use the open-source sympy solver (CITE) to convert the system into a set of first-order ODEs to make solution numerically tractable.

We the thermodynamic model tracks the temperatures and the core mantle boundary and upper-mantle, while the chemical equations track the number of moles of four species in the core and five in the interaction layer. This gives a state vector $\mathbf{x}$ with eleven components. We specify the initial state by setting $T_{CMB,0}$ and $T_{UM,0}$ as well as the initial composition of the core $M_{Fe}, M_{Mg}, M_{Si}, M_O$. This sets the initial interaction layer composition by requiring it be in equilibrium with the core at formation. We find that many initial core compositions require initial interaction layer compositions very different from what we expect at the present day. In particular, many initial compositions require a layer highly enriched in ferropericlase. Thus, we adjust the equlibrium constant governing the Bridgemanite to ferropericlase ratio towards the expected present-day value on the same timescale τ as mantle overturn. Finally, we solve the complete system of equations forward in time from formation to the presnt day using scipy's built-in ODEint solver.

4 Results

Using this model, we can compute a self-consistent evolution of the composition and thermal state of Earth's core and mantle over time. We show in figure 2 the evolution of Earth for an initial CMB temperature 5750K; initial core composition 0.5 wt% Mg and Si, 1.5 wt% O; interaction layer thickness 100m; present-day mantle overturn time 400 Myr; and present-day mantle viscosity 10^{21}Pa-s. In this history, entropy production is initially dominated by secular cooling before FeO begins to exsolve out of the core and becomes the dominant source of entropy production. Then, as the core cools, both SiO2 and MgO begin to exsolve at distinct times, causing small spikes in total entropy available but contributing less to the overall entropy budget than either FeO or secular cooling. For the $\sim$2 Byrs before inner-core nucleation, secular cooling is the largest single contributor to the entropy budget, but exsolution of light elements still produces a significant amount of entropy. Inner-core nucleation brings a powerful new source of entropy production which causes a spike in total available entropy for the dynamo and depresses the core cooling rate. This causes entropy production from cooling and exsolution to decline and allows inner-core entropy production to dominate all other sources to the present day.

In this history, the mantle interaction layer is significantly enriched in iron in the early Earth, with a Mg# ~ 0.25 (see fig. 2d). As exsolution slows near

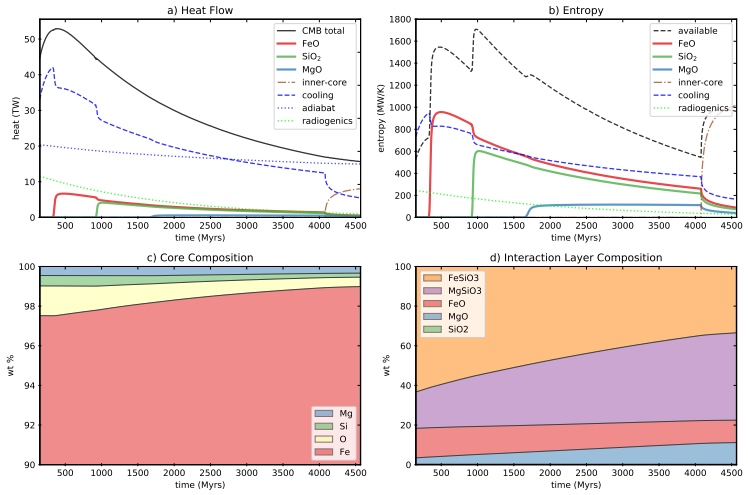

Figure 2: Overview of the dynamics and reactions governing chemical exchange between the core and mantle.

the present day, the enriched layer is swept away as material is incorporated from background mantle convection increasing the Mg# to ∼0.6. The layer is still enriched in iron at the present day compared to the background mantle, which has a Mg# ∼0.8. This has possible implications for the origin of LLSVPs and ULVZs, as mantle convection could collect dense material near the base of upwellings and plumes as LLSVPs or sweep material into piles to form ULVZs [TODO:CITE].

Table 2: Model Variables

Parameter	Description	Range	Units
$w_{Mg,0}$	initial Mg wt% in core	10^{-5} - TODO	-
$w_{Si,0}$	initial Si wt% in core	10^{-5} - TODO	-
$w_{O,0}$	initial O wt% in core	10^{-5} - TODO	-
$T_{CMB,0}$	initial core-mantle boundary temperature	5000 - 6250	K
H	interaction layer thickness	30 - 1000	m
μ_p	present-day mantle viscosity	$10^{19.5}$ - 10^{21}	Pa-s
τ_p	present-day mantle overturn timescale	200 - 800	Myrs

4.1 Entropy Production Over Time

We run a suite of parameters using our model, varying the values listed in table 1 and keeping runs that have result in a present-day inner-core size within 10% of the real value. We show entropy histories of runs that match present-day observations in figure 3. We color the histories by the dominant entropy production mechanism, with blue lines denoting secular cooling, red lines denoting

FeO exsolution, and green lines denoting SiO2 exsolution. Figure 3a shows the entropy available to power a dynamo, demonstrating a huge variety of possible histories, but with some general trends visible.

Nearly all runs have FeO exsolution as the largest source of compositional entropy production, as can be seen in fig. 3b and the color of lines in fig 3a. FeO exsolution produces 50-100% of all compostional entropy in the early earth, and 40-100% just before inner-core nucleation (figure 3b). In some histories MgO or SiO2 breifly produce more entropy that FeO, but in almost all histories FeO is the largest single source of compositional entropy production through the majority of Earth's history. However, after the inner core begins to grow, FeO exsolution becomes much less important, contributing less than 10% of the compositional entropy budget at the present day in most histories.

In general the total amount of entropy available for a dynamo is largest in the early earth, declines to a minimum in the $\sim$ billion years before inner-core nucleation, then increases suddenly with inner core nucleation and remains strong to the present day.

Secular cooling is the sole source of entropy production before inner-core nucleation, in a few histories (fig. 3c). However, even runs dominated by secular cooling usually have some amount of exsolution. Many histories show that entropy production is initially dominated by cooling before one or more elements begin to exsolve from the core and become the dominant source of entropy (see fig. 3c). Over time, cooling produces a steadily greater fraction of total entropy until it contributes 30-75% of total entropy just before inner-core nucleation. After inner-core nucleation, it diminishes in importance and produces $\sim$15% of total entropy at the present day.

4.2 Inner-Core Nucleation

We use our suite of histories to examine how exsolution affects the timing of and change in entropy production with inner core nucleation. We detail the evolution of available entropy near inner-core nucleation in fig. 4a, showing that all histories experience a positive jump in available entropy after nucleation.

The magnitude of the jump in entropy available varies between histories, and is significantly affected by the presence of exsolution. For histories with cooling as the dominant source of entropy production, the the median increase in available entropy is $\sim 140\%$, (fig. 4b) which might be expected to produce an observable signal in paleointensity records (Olson and Christensen 2006) which past authors have claimed to detect (e.g. Biggin et al. 2015). However, histories with exsolution as the dominant source of entropy production have a median entropy increase of $\sim 60\%$, reducing the size of the increase by more than half and making detection in the paleomagnetic record less likely. In addition, the change in the dominant entropy production mechanism from exsolution at the CMB to inner-core growth at the center of the core might reduce how much available entropy is expressed as magnetic field observable at Earth's surface (Landeau, Aubert, Olson 2017), further reducing the size of the paleomagnetic signal. This is potentially consistent with recent results arguing for a relatively

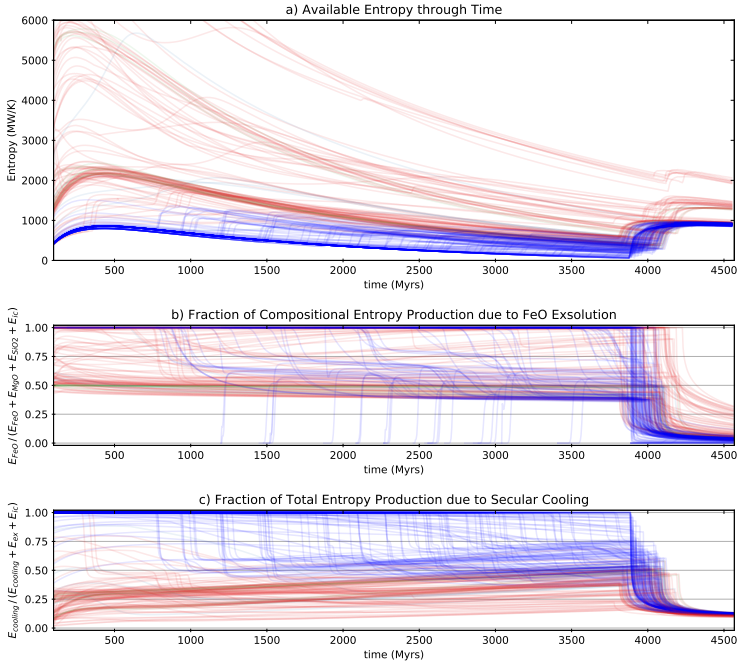

Figure 3: Overview of the dynamics and reactions governing chemical exchange between the core and mantle.

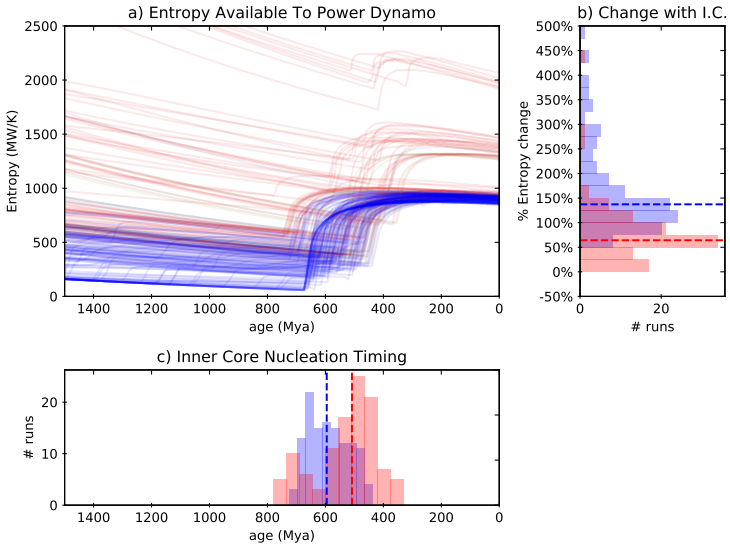

Figure 4: Inner-core nucleation signals and timing. (a) shows total entropy available in all valid runs, (b) is histogram of percentage increase in available entropy from 1 Myr before to 100 Myr after inner-core nucleation, with median $\sim$ 100% increase. (c) shows a histogram of inner-core nucleation times, with median $\sim$ 600 Mya.

constant observed field strength for the last 1.5 Byrs (Sprain 2018).

Exsolution also increases the variance in inner-core nucleation timing (fig 4c). Dynamos powered by cooling have a inner-core nucleation ages varying from $\sim$540 to $\sim$700 Mya, with a median age of $\sim$600 Myrs. Exsolution expands the range to $\sim$350 to $\sim$760 Mya and decreases the median age to $\sim$500 Myrs. Neither of these reuslts are significantly different from those obtained by Nimmo (2015), as might be expected since we use a modified form of his core parameterization.

5 Conclusions

FeO exsolution is an important source of entropy to power Earth's dynamo. Exsolution of light elements from Earth's core is governed by the composition of the lowermost mantle and the timescale of mantle dynamics.

References

James Badro, Julien Siebert, and Francis Nimmo. An early geodynamo driven by exsolution of mantle components from Earth's core. *Nature*, 536(7616):

1–3, 2016. ISSN 1098-6596. doi: 10.1017/CBO9781107415324.004. URL http://dx.doi.org/10.1038/nature18594.

Craig R. Bina. Scale limits of free-silica seismic scatterers in the lower mantle. *Physics of the Earth and Planetary Interiors*, 183(1-2):110–114, 2010. ISSN 00319201. doi: 10.1016/j.pepi.2010.06.008.

Leslie A. Hayden and E. Bruce Watson. A diffusion mechanism for core-mantle interaction. *Nature*, 450(7170):709–711, 2007. ISSN 14764687. doi: 10.1038/nature06380.

George Helffrich, Maxim Ballmer, and Kei Hirose. Core-exsolved S i O ₂ dispersal in the Earth's mantle. *Journal of Geophysical Research: Solid Earth*, pages 176–188, 2017. ISSN 21699313. doi: 10.1002/2017JB014865. URL http://doi.wiley.com/10.1002/2017JB014865.

Kei Hirose, Guillaume Morard, Ryosuke Sinmyo, Koichio Umemoto, John Hernlund, George Helffrich, and Stéphane Labrosse. Crystallization of silicon dioxide and compositional evolution of the Earth's core. *Nature*, 543(7643):99–102, 2017. ISSN 14764687. doi: 10.1038/nature21367.

Ravi V.S. Kanda and David J. Stevenson. Suction mechanism for iron entrainment into the lower mantle. *Geophysical Research Letters*, 33(2):4–7, 2006. ISSN 00948276. doi: 10.1029/2005GL025009.

Stéphane Labrosse. Thermal evolution of the core with a high thermal conductivity. *Physics of the Earth and Planetary Interiors*, 247:36–55, 2015. ISSN 00319201. doi: 10.1016/j.pepi.2015.02.002. URL http://linkinghub.elsevier.com/retrieve/pii/S0031920115000175.

F Nimmo. *Energetics of the Core*. Elsevier B.V., 2015. doi: 10.1016/B978-0-444-53802-4.00139-1. URL http://dx.doi.org/10.1016/B978-0-444-53802-4.00139-1.

Joseph G. O'Rourke and David J. Stevenson. Powering Earth's dynamo with magnesium precipitation from the core. *Nature*, 529(7586):387–389, jan 2016. ISSN 0028-0836. doi: 10.1038/nature16495. URL http://www.nature.com/doifinder/10.1038/nature16495.

Monica Pozzo, Chris Davies, David Gubbins, and Dario Alfè. Thermal and electrical conductivity of iron at Earth's core conditions. *Nature*, 485(7398):355–358, 2012. doi: 10.1038/nature11031. URL http://adsabs.harvard.edu/cgi-bin/nph-data{_}query?bibcode=2012Natur.485..355P{&}link{_}type=ABSTRACT.

David J Stevenson, Tilman Spohn, and Gerald Schubert. Magnetism and thermal evolution of the terrestrial planets. *Icarus*, 54(3):466–489, 1983. doi: 10.1016/0019-1035(83)90241-5. URL

http://adsabs.harvard.edu/cgi-bin/nph-data{_}query?bibcode=1983Icar...54..466S{&}link{_}type=ABSTRACT.

J A Tarduno, R D Cottrell, W J Davis, F Nimmo, and R K Bono. A Hadean to Paleoarchean geodynamo recorded by single zircon crystals. *Science*, 2015. URL http://www.sciencemag.org/content/349/6247/521.short.

James A. Van Orman, Yingwei Fei, Erik H. Hauri, and Jianhua Wang. Diffusion in MgO at high pressures: Constraints on deformation mechanisms and chemical transport at the core-mantle boundary. *Geophysical Research Letters*, 30(2):26–29, 2003. ISSN 00948276. doi: 10.1029/2002GL016343. URL http://doi.wiley.com/10.1029/2002GL016343.